ELSEVIER

Journal of Organometallic Chemistry 580 (1999) 313–319

Journal of Organometallic Chemistry

Synthesis and structural characterization of $Mo_2(\mu\text{-}SC_6H_4\text{–}Cl\text{-}p)_2(\mu\text{-}dppm)(CO)_6$ and $[(dppm)(CO)_2Mo(\mu\text{-}SC_6H_4\text{–}Cl\text{-}p)_2Mo(O)]_2(\mu\text{-}SC_6H_4\text{–}Cl\text{-}p)_2(\mu\text{-}O)$ and electrochemical property of $Mo_2(\mu\text{-}SC_6H_4\text{–}Cl\text{-}p)_2(\mu\text{-}dppm)(CO)_6$

Guohua Pan, Botao Zhuang *, Lingjie He, Jiutong Chen, Jiaxi Lu

State Key Laboratory of Structural Chemistry, Fujian Institute of Research on the Structure of Matter, Chinese Academy of Sciences, Fuzhou, Fujian 350002, PR China

Received 28 September 1998

Abstract

Dimolybdenum(I) compound $Mo_2(\mu\text{-}SC_6H_4\text{–}Cl\text{-}p)_2(\mu\text{-}dppm)(CO)_6$ (**1**), ($dppm = (C_6H_5)_2PCH_2P(C_6H_5)_2$), and a trace unexpected mixed-valence tetranuclear molybdenum compound $[(dppm)(CO)_2Mo(\mu\text{-}SC_6H_4\text{–}Cl\text{-}p)_2Mo(O)]_2(\mu\text{-}SC_6H_4\text{–}Cl\text{-}p)_2(\mu\text{-}O)$ (**2**) were obtained from the reaction of $Mo_2(\mu\text{-}SC_6H_4\text{–}Cl\text{-}p)_2(CO)_8$ with dppm in CH_2Cl_2. The crystal structures of the two compounds have been determined by X-ray diffraction studies. **1**: monoclinic, $P2(1)/n$, $a = 13.1082(3)$, $b = 23.9584(4)$, $c = 14.8510(2)$ Å, $\beta = 105.865(1)°$, $V = 4486.32(14)$ Å^3, $Z = 4$, 9859 unique data, $R_1 = 0.0805$, $wR_2 = 0.1076$. **2**·CH_2Cl_2: monoclinic, $C2/c$, $a = 22.0955(13)$, $b = 19.1563(11)$, $c = 25.1981(14)$ Å, $\beta = 112.243(1)°$, $V = 9871.9(1)$ Å^3, $Z = 4$, 7053 unique data, $R_1 = 0.0450$, $wR_2 = 0.1222$. The cyclic voltammetry (CV) measurement for **1** showed a reversible two-electron transfer in a single step.

Keywords: Molybdenum; Mo_2S_2 unit; Crystal structure; Electrochemistry

1. Introduction

We are continuously interested in the research on low-valence dinuclear molybdenum carbonyl thiolate compounds $[Mo_2(\mu\text{-}SR)_2(CO)_8]^{2-,0}$ (R = Ph [1,2], CH_2CO_2Et [3], *o*-$H_3C\text{–}C_6H_4$ [4]), because they possess an interesting two-electron transfer character in a single step when containing a planar Mo_2S_2 unit and lose this electrochemical feature when containing a butterfly type Mo_2S_2 core [4]. Studies on this kind of compound were mainly focused on Mo(0) atom, however, less Mo(I) compounds were systematically investigated. More recently, an attempt to further develop studies on synthesis, structure and physical and chemical properties of rare Mo(I) carbonyl thiolate compound has been carried out in this research group. By reaction of $Mo_2(\mu\text{-}SC_6H_4\text{–}Cl\text{-}p)_2(CO)_8$ with dppm, a new dinuclear molybdenum(I) carbonyl thiolate compound with a diphosphine bridging ligand $Mo_2(\mu\text{-}SC_6H_4\text{–}Cl\text{-}p)_2(\mu\text{-}dppm)(CO)_6$ (**1**) and a by-product $[(dppm)(CO)_2Mo(\mu\text{-}SC_6H_4\text{–}Cl\text{-}p)_2Mo(O)]_2(\mu\text{-}SC_6H_4\text{–}Cl\text{-}p)_2(\mu\text{-}O)$ (**2**) have been obtained and investigated. Herein, we report the synthesis and structural characterization of **1** and **2**, and electrochemical behavior of **1**.

* Corresponding author. Fax: +86-0591-3714946.
E-mail address: zbt@ms.fjirsm.ac.cn (B. Zhuang)

0022-328X/99/$ - see front matter
PII: S0022-328X(98)01168-1

2. Results and discussion

2.1. Syntheses and characterization

Reaction of $Mo_2(\mu\text{-}SC_6H_4\text{–}Cl\text{-}p)_2(CO)_8$ with dppm in dichloromethane yielded dinuclear compound, $Mo_2(\mu\text{-}SC_6H_4\text{–}Cl\text{-}p)_2(\mu\text{-dppm})(CO)_6$ (**1**), and a trace of tetranuclear compound, $[(dppm)(CO)_2Mo(\mu\text{-}SC_6H_4\text{–}Cl\text{-}p)_2Mo(O)]_2(\mu\text{-}SC_6H_4\text{–}Cl\text{-}p)_2(\mu\text{-O})$ (**2**), which were separated as red crystals under a microscope. But reaction of $Mo_2(\mu\text{-}SC_6H_4\text{–}Cl\text{-}p)_2(CO)_8$ with Bu_4NBr and then dppm in acetone only afforded compound **1** in high yield. The compound **1** has been characterized by spectroscopies and elemental analysis.

The IR spectrum of **1** exhibited five ν(CO) bands at 2010, 1963, 1934, 1917, 1884 cm^{-1}. The ^{1}H-NMR and ^{13}C-NMR spectra of **1** showed peaks at 2.9 and 55.1 ppm, respectively, which were attributed to CH_2 in P–CH_2–P of dppm, indicating dppm coordinating to the parent compound $Mo_2(\mu\text{-}SC_6H_4\text{–}Cl\text{-}p)_2(CO)_8$. The only ^{31}P-NMR peak at 18.4 ppm observed for **1** indicated each P atom coordinating to central metal atom is in identical electron structure and coordination environment. Likewise, the only ^{95}Mo-NMR peak at -936 ppm also indicated that the electronic structure and the space structure of the two molybdenum atoms are identical. The ^{95}Mo-NMR chemical shift of compound **1** is more downfield than that of $Mo_2(\mu\text{-}SC_6H_4\text{–}Cl\text{-}p)_2(CO)_8$ (-1100 ppm), indicating that coordination of dppm leads to more deshielding than that of CO. This is consistent with the results: in general substitution of a CO group in $Mo(CO)_6$ by a weaker π-acceptor than CO leads to deshielding relative to $Mo(CO)_6$, reported by Minelli et al. [5]. It seems that this result is contrary to the general idea that substituting CO by dppm should lead to increasing electron density on metal atom, but considering the chemical shift–oxidation state relationship that holds in the di- and tri-nuclear Mo–W-series complexes with an M–M bond: the shielding increases (NMR signal shift to upfield) with an increase in oxidation state [6,7] this result is comprehensible. The compound **2** was characterized by measurement of IR and ^{31}P-NMR spectra because only a few single crystals were obtained. The IR spectrum of **2** showed two ν(CO) bands at 1888 and 1869 cm^{-1}, which had a red shift relative to that of **1**; this might be attributed to the increase of metal–CO back-donating when a P atom replaces CO. In addition, the absorption at 910 cm^{-1} is characteristic of terminal Mo=O and the peak at 748 cm^{-1} should be the vibration of Mo–O–Mo [8]. The only ^{31}P-NMR at 9.7 ppm of **2** is more upfield than that of **1**, indicating the different coordinating pattern of dppm between **1** and **2**. In fact, as shown in below structure analyses, the coordinating mode of dppm in **1** and **2** are interbridging and chelating, respectively [9].

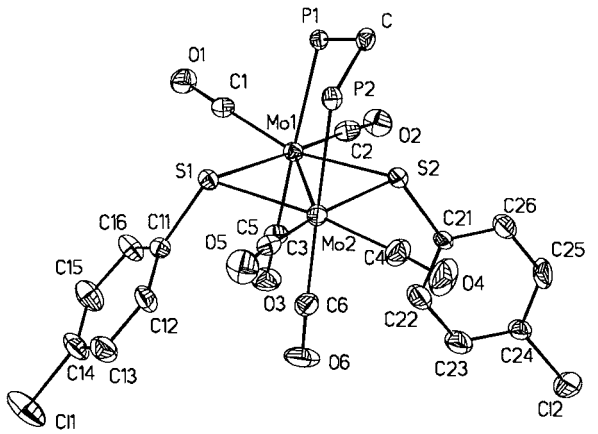

Fig. 1. A view of a molecule of **1** with 30% probability ellipsoids. The phenyl rings of dppm are omitted.

2.2. Crystal structures

2.2.1. The structure of *1*

The structure of **1** is shown in Fig. 1. Selected bond lengths and bond angles are listed in Table 1. The molecule of **1** consists of two *fac*-$Mo(CO)_3$ fragments linked by an Mo–Mo bond, two *p*-chrolo-phenylthiolate bridging groups and a bidentate bridging dppm ligand. The geometry of each Mo atom is distorted octahedron with 3C, 1P, and 2S. The distortion is due to the large SMoS angle of 105.70(3)°. Two bridging S atoms and two carbonyl groups form an equatorial plane, the other carbonyl and the P atom of dppm ligand occupy the axial position of each Mo atom. The whole structure could be considered as an edge-sharing bioctahedral structure consisting of two distorted octahedrons with central Mo atoms in which the Mo–Mo bond length is 2.9946(10) Å, indicating the metal–metal

Table 1
Selected bond lengths(Å) and angles (°) for **1**

Mo(1)–C(3)	1.989(10)	Mo(2)–C(4)	2.026(10)
Mo(1)–C(2)	2.003(10)	Mo(2)–S(2)	2.484(2)
Mo(1)–C(1)	2.006(9)	Mo(2)–S(1)	2.491(2)
Mo(1)–S(2)	2.459(2)	Mo(2)–P(2)	2.571(3)
Mo(1)–S(1)	2.499(2)	C(1)–O(1)	1.144(8)
Mo(1)–P(1)	2.563(2)	C(2)–O(2)	1.149(9)
Mo(1)–Mo(2)	2.9946(10)	C(3)–O(3)	1.150(10)
Mo(2)–C(6)	1.972(12)	C(4)–O(4)	1.126(9)
Mo(2)–C(5)	2.000(10)	C(5)–O(5)	1.151(9)
		C(6)–O(6)	1.147(11)
S(2)–Mo(1)–S(1)	105.96(7)	S(1)–Mo(2)–P(2)	90.32(7)
S(2)–Mo(1)–P(1)	81.62(7)	S(2)–Mo(2)–Mo(1)	52.34(5)
S(1)–Mo(1)–P(1)	95.13(7)	S(1)–Mo(2)–Mo(1)	53.25(5)
S(2)–Mo(1)–Mo(2)	53.10(5)	P(2)–Mo(2)–Mo(1)	90.00(5)
S(1)–Mo(1)–Mo(2)	53.00(5)	Mo(2)–S(1)–Mo(1)	73.75(6)
P(1)–Mo(1)–Mo(2)	90.57(5)	Mo(1)–S(2)–Mo(2)	74.57(6)
S(2)–Mo(2)–S(1)	105.44(7)	P(2)–C–P(1)	111.4(4)
S(2)–Mo(2)–P(2)	85.76(8)		

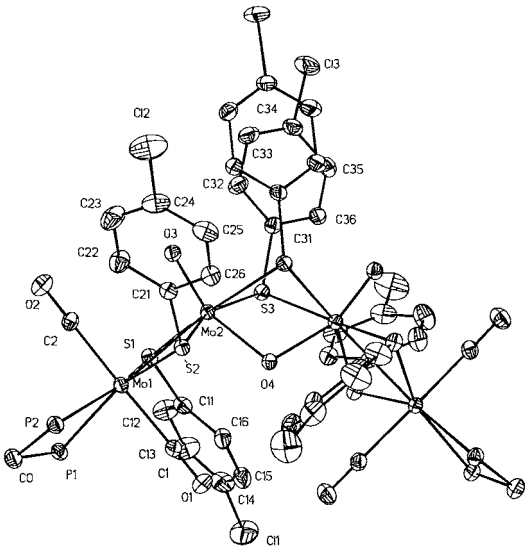

Fig. 2. A view of a molecule of **2** with 30% probability ellipsoids. The phenyl rings of dppm are omitted.

interaction that results from the coupling of the unpaired spins of two Mo(I) ions (d^5). The bond distance of Mo(1)–S(1) (2.499(2) Å) is slightly longer than that of Mo(1)–S(2)(2.459(2) Å). The Mo_2S_2 unit is planar, and, in contrast with $Mo_2(\mu\text{-}SPh)_2(CO)_8$ [10], the two benzene rings of thiolates are in *syn* orientation relative to the Mo_2S_2 plane. This is due to the great hindrance of dppm ligand. The axial Mo–C (*trans* to dppm) (mean 1.980(10) Å) is slightly shorter than the equatorial Mo–C (*trans* to S bridging) (mean 2.009(10) Å) because of the *trans*-effect of dppm and *p*-chrolophenylthiolato ligand. The shorter axial Mo–C length and the steric hindrance from the *syn* orientation of *p*-chrolophenylthiolato ligands imply a difficulty to obtain four-bridge compound, $Mo_2(\mu\text{-}SC_6H_4\text{–}Cl\text{-}p)_2(\mu\text{-dppm})_2(CO)_4$. P–Mo–Mo angle is near 90°, P–C–P angle is 111.4(4)°, the span of two P atoms of dppm is just matching the Mo–Mo bond length. It is obvious that **1** forms via a substitution of a dppm for the two axial carbonyl groups which are on the same side with respect to Mo_2S_2 plane in the parent compound $Mo_2(\mu\text{-}SC_6H_4\text{–}Cl\text{-}p)_2(\mu\text{-dppm})(CO)_6$.

2.2.2. The structure of *2*

The structure of **2** is shown in Fig. 2. Selected bond lengths and angles are listed in Table 2. The molecule of **2** can be viewed as the structure that two species $[(dppm)(CO)_2Mo(\mu\text{-}SC_6H_4\text{–}Cl\text{-}p)_2Mo(O)]$ linked by two bridging SC_6H_4–Cl-*p* and one bridging oxo, or two fragments $[(dppm)(CO)_2Mo(\mu\text{-}SC_6H_4\text{–}Cl\text{-}p)_2]$ connected with $(O)Mo(\mu\text{-}SC_6H_4\text{–}Cl\text{-}p)_2(\mu\text{-}O)Mo(O)$ core. A c_2 axis is passing through the bridging oxygen atom, and the carbon atom of solvent molecule CH_2Cl_2 is also located on this axis.

Table 2
Selected bond lengths (Å) and angles (°) for **2**·CH_2Cl_2[a]

Mo(1)–C(2)	2.009(6)	Mo(2)–S(2)	2.4623(14)
Mo(1)–C(1)	2.028(6)	Mo(2)–S(1)	2.4623(14)
Mo(1)–S(1)	2.407(2)	Mo(2)–S(3) # 1	2.5682(14)
Mo(1)–S(2)	2.4158(14)	Mo(2)–S(3)	2.5911(14)
Mo(1)–P(2)	2.500(2)	S(3)–Mo(2) # 1	2.5682(14)
Mo(1)–P(1)	2.501(2)	O(1)–C(1)	1.136(7)
Mo(1)–Mo(2)	2.8570(6)	O(2)–C(2)	1.144(7)
Mo(2)–O(3)	1.699(4)	O(4)–Mo(2) # 1	1.980(3)
Mo(2)–O(4)	1.980(3)	Mo(2)–Mo(2) # 1	3.250(3)
S(1)–Mo(1)–S(2)	109.72(5)	S(1)–Mo(2)–S(3) # 1	166.59(5)
S(1)–Mo(1)–P(2)	154.35(5)	O(3)–Mo(2)–S(3)	94.18(13)
S(2)–Mo(1)–P(2)	95.26(5)	O(4)–Mo(2)–S(3)	72.49(9)
S(1)–Mo(1)–P(1)	89.30(5)	S(2)–Mo(2)–S(3)	160.95(5)
S(2)–Mo(1)–P(1)	157.49(5)	S(1)–Mo(2)–S(3)	82.34(5)
P(2)–Mo(1)–P(1)	67.79(5)	S(3) # 1–Mo(2)–S(3)	84.49(5)
S(1)–Mo(1)–Mo(2)	54.98(3)	O(3)–Mo(2)–Mo(1)	99.50(12)
S(2)–Mo(1)–Mo(2)	54.91(3)	O(4)–Mo(2)–Mo(1)	101.44(12)
P(2)–Mo(1)–Mo(2)	148.64(4)	S(2)–Mo(2)–Mo(1)	53.40(3)
P(1)–Mo(1)–Mo(2)	143.56(4)	S(1)–Mo(2)–Mo(1)	53.17(4)
O(3)–Mo(2)–O(4)	159.0(2)	S(3) # 1–Mo(2)–Mo(1)	138.83(4)
O(3)–Mo(2)–S(2)	101.96(13)	S(3)–Mo(2)–Mo(1)	133.89(4)
O(4)–Mo(2)–S(2)	89.09(8)	Mo(1)–S(1)–Mo(2)	71.85(4)
O(3)–Mo(2)–S(1)	93.58(13)	Mo(1)–S(2)–Mo(2)	71.69(4)
O(4)–Mo(2)–S(1)	100.45(7)	C(31)–S(3)–Mo(2) # 1	109.7(2)
S(2)–Mo(2)–S(1)	106.41(5)	C(31)–S(3)–Mo(2)	119.9(2)
O(3)–Mo(2)–S(3) # 1	89.89(13)	Mo(2) # 1–S(3)–Mo(2)	78.15(4)
O(4)–Mo(2)–S(3) # 1	73.03(9)	Mo(2) # 1–O(4)–Mo(2)	110.4(2)
S(2)–Mo(2)–S(3) # 1	85.48(4)	P(2)–C(0)–P(1)	98.8(3)

[a] Symmetry transformations used to generate equivalent atoms: # 1, $-x+1, y, -z+1/2$; # 2, $-x, y, -z+1/2$.

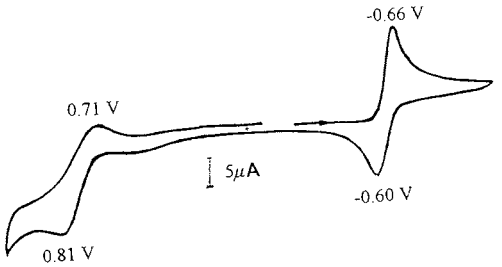

Fig. 3. Cyclic voltammograms of **1**, recorded in acetone; concentration, 0.0002 M; scan rate, 100 mV s^{-1}.

In the half of the structure of **2**, the coordination environments and the oxidation states of two Mo atoms are different. The Mo(1) atom, in +1 oxidation state, is located in a distorted octahedron with 2P, 2S and 2CO groups, having a large S(1)Mo(1)S(2) angle (109.72(5)°) and small P(1)Mo(1)P(2) angle (67.79(5)°). Mo(1)–C(1) (2.028(6) Å) is 0.02 Å longer than Mo(1)–C(2) (2.009(6) Å). The PCP angle is 98.8(3)°. The dppm acts as a chelate ligand in accordance with the datum observed on ^{31}P-NMR. But the Mo(2) atom, in +5 oxidation state, is in six coordination with 2O and 4S, of which the geometry of Mo(2) atom cannot be described in terms of simple symmetry. Mo(1), Mo(2), S(1), and S(2) atoms are coplanar. Relative to the Mo_2S_2 plane, two benzene rings of thiolates are in anti orientation in contrast with that of **1**. The Mo(1)–Mo(2) length of 2.8570(6) Å is somewhat shorter than that of **1**, due to the high oxidation state of Mo(2). The metal–metal bonding resulted from the coupling of the unpaired spins of one Mo(I) and one Mo(V) (d^1–d^5). The Mo(2)–Mo(2#) distance is 3.250(3) Å, indicating no metal–metal interaction between Mo(2) and Mo(2#). Because of dppm *trans*-effect, both Mo(1)–S(1) and Mo(1)–S(2) become shorter than those of **1**; in addition, Mo(1)–S(1) (2.407(2) Å) is ca. 0.01 Å shorter than Mo(1)–S(2) (2.4158(14) Å). Mo(2)=O bond length (1.699(4) Å) and Mo(2)–O(4) (1.980(3) Å) are in the normal ranges [8,11].

The formation mechanism of the tetranuclear oxo-product [(dppm)$(CO)_2$Mo(μ-SC_6H_4–Cl-*p*)$_2$Mo(O)]$_2$(μ-SC_6H_4–Cl-*p*)$_2$(μ-O) (**2**) could not be ascertained, but we assume that the trace oxygen comes from an unexpected leakage in the course of experiment. In fact, the oxidation of Mo(2) atom from +1 to +5 also could manifest this phenomenon. However, the addition of air to the reaction mixture does not improve the yield of **2** significantly implying that the formation of **2** dose not come from the oxidation of **1** and, however, the presence of dioxygen leads to extensive degradation of **1** and complicated oxo-products.

2.3. Electrochemical behavior

The cyclic voltammogram of **1** is depicted in Fig. 3. Compound **1** displays a reversible redox couple at −0.63 V (−0.60/−0.66 V vs. SCE) and redox peaks

Table 3
Crystallographic data for **1** and **2**·CH_2Cl_2

Compound	**1**	**2**·CH_2Cl_2
Empirical formula	$C_{43}H_{30}Cl_2Mo_2O_6P_2S_2$	$C_{91}H_{70}Cl_8Mo_4O_7P_4S_6$
Formula weight	1031.51	2259.07
Crystal system	Monoclinic	Monoclinic
Space group	*P*2(1)/*n*	*C*2/*c*
a (Å)	13.1082(3)	22.0955(13)
b (Å)	23.9584(4)	19.1563(11)
c (Å)	14.8510(2)	25.1981(14)
β (°)	105.865(1)	112.243(1)
V (Å^3), *Z*	4486.32(14), 4	9871.9(1), 4
$D_{calc.}$ (Mg m^{-3})	1.527	1.520
λ (mm^{-1})	0.887	0.955
Min/max transmission	0.928/0.694	0.943/0.715
F(000)	2064	4528
Crystal size (mm^3)	0.24×0.10×0.10	0.20×0.15×0.10
θ range (°)	1.66–25.03	1.49–23.26
Index ranges	$-10 \le h \le 15$	$-22 \le h \le 24$
	$-20 \le k \le 28$	$-21 \le k \le 19$
	$-17 \le l \le 13$	$-27 \le l \le 17$
Reflections collected	16140	18920
Independent reflections	7895	7053
Data/restraints/parameters	7806/0/514	7053/0/542
R_1, wR_2 [$I>2\sigma(I)$]	0.0805, 0.1076	0.0450, 0.1222
R_1, wR_2 [all data]	0.1823, 0.2367	0.0575, 0.1333
Goodness-of-fit	1.150	1.064
Largest difference peak/hole (e Å^{-3})	0.554/−0.707	1.743/−0.462

Table 4
Atomic coordinates ($\times 10^4$) and equivalent isotropic displacement parameters (Å $\times 10^3$) for **1**

Atom	x	y	z	U_{eq}
Mo(1)	−1175(1)	4067(1)	5480(1)	41(1)
Mo(2)	−2284(1)	2966(1)	5043(1)	44(1)
S(1)	−3037(2)	3904(1)	4518(2)	42(1)
S(2)	−483(2)	3147(1)	6091(2)	46(1)
Cl(1)	−3873(3)	4348(2)	201(2)	144(2)
Cl(2)	3413(2)	2126(1)	4956(2)	102(1)
P(1)	−1636(2)	4108(1)	7048(2)	39(1)
P(2)	−2923(2)	3048(1)	6528(2)	45(1)
C	−1988(6)	3431(3)	7463(6)	46(2)
C(1)	−1526(7)	4883(4)	5381(6)	46(2)
C(2)	308(8)	4298(4)	6145(7)	55(3)
C(3)	−713(7)	4075(4)	4311(7)	50(2)
C(4)	−1872(8)	2157(4)	5322(7)	71(3)
C(5)	−3697(8)	2639(4)	4392(7)	57(3)
C(6)	−1838(7)	2864(4)	3889(8)	62(3)
C(11)	−3204(7)	4014(3)	3303(6)	45(2)
C(12)	−3743(7)	3640(4)	2647(7)	65(3)
C(13)	−3951(8)	3744(4)	1693(8)	76(3)
C(14)	−3626(9)	4232(6)	1392(7)	79(3)
C(15)	−3101(8)	4611(5)	2032(8)	83(3)
C(16)	−2892(7)	4499(4)	2980(7)	63(3)
C(21)	619(6)	2890(3)	5712(6)	44(2)
C(22)	698(9)	2893(5)	4817(8)	117(5)
C(23)	1556(9)	2654(6)	4582(8)	111(5)
C(24)	2349(7)	2435(4)	5242(7)	60(3)
C(25)	2331(8)	2468(5)	6118(9)	102(4)
C(26)	1471(8)	2712(4)	6373(7)	81(3)
C(111)	−529(6)	4344(3)	7996(6)	42(2)
C(112)	15(8)	4014(4)	8727(8)	82(3)
C(113)	871(10)	4218(6)	9416(9)	121(5)
C(114)	1172(9)	4758(6)	9388(9)	101(4)
C(115)	659(9)	5092(5)	8697(9)	86(4)
C(116)	−179(8)	4890(4)	8011(7)	67(3)
C(121)	−2700(7)	4568(3)	7186(6)	43(2)
C(122)	−2756(7)	4729(4)	8067(7)	62(3)
C(123)	−3537(8)	5072(4)	8184(8)	77(3)
C(124)	−4311(8)	5258(4)	7400(9)	72(3)
C(125)	−4286(7)	5100(4)	6538(8)	68(3)
C(126)	−3474(7)	4768(3)	6413(6)	52(2)
C(211)	−4210(7)	3353(3)	6516(7)	49(2)
C(212)	−4945(8)	3488(4)	5691(7)	60(3)
C(213)	−5923(9)	3717(4)	5675(9)	81(4)
C(214)	−6150(9)	3813(5)	6489(11)	95(4)
C(215)	−5454(10)	3686(5)	7329(10)	107(4)
C(216)	−4484(8)	3450(4)	7334(8)	81(3)
C(221)	−2971(8)	2364(3)	7059(6)	49(2)
C(222)	−3903(8)	2075(4)	6932(7)	77(3)
C(223)	−3912(11)	1535(5)	7269(9)	110(5)
C(224)	−2985(13)	1281(5)	7737(9)	103(5)
C(225)	−2064(10)	1561(4)	7892(8)	91(4)
C(226)	−2049(8)	2094(4)	7542(7)	69(3)
O(1)	−1746(5)	5347(3)	5343(5)	71(2)
O(2)	1176(5)	4419(3)	6488(5)	78(2)
O(3)	−422(5)	4104(3)	3649(5)	81(2)
O(4)	−1632(6)	1705(3)	5422(6)	116(3)
O(5)	−4471(6)	2421(3)	3995(6)	92(3)
O(6)	−1591(7)	2780(4)	3218(6)	115(3)

at 0.81 and 0.71 V versus SCE. The peak current parameter ($i_p/V^{1/2}AC$) of the event at −0.66 V is 1321 A $V^{-1/2}$ $s^{1/2}$ cm mol^{-1}, which is nearly double that of ferrocene (690 A $V^{-1/2}$ $s^{1/2}$ cm mol^{-1}) observed under identical conditions (ferrocene was used as an internal potential standard). This implies that like the electrochemical behavior of $[Mo_2(SPh)_2(CO)_8]$ and its bisubstituted product, $[Mo_2(SPh)_2(CO)_6(MeCN)_2]$ [1,2], compound **1** undergoes two-electron reversible reduction in a potential at −0.63V as shown in Eq. (1).

$$[Mo_2(SC_6H_4Cl)_2(dppm)(CO_6)]^0 \overset{-0.63\ V}{\underset{2\ e}{\rightleftharpoons}} [Mo_2(SC_6H_4Cl)_2(dppm)(CO_6)]^{2-} \quad (1)$$

The existence of similar electrochemical behavior between compound **1** and $[Mo_2(SPh)_2(CO)_8]$ and $[Mo_2(SPh)_2(CO)_6(MeCN)_2]$ is reasonable because they have a common planar M_2S_2 unit. Similar to the bisubstituted product, $[Mo_2(SPh)_2(CO)_6(MeCN)_2]$, compound **1** underwent two-electron reversible reduction at more negative potential than the parent analog $[Mo_2(SPh)_2(CO)_8]$ (−0.4 V vs. SCE) [1,2] and the redox couple potential of compound **1** is more positive than that of $[Mo_2(SPh)_2(CO)_6(MeCN)_2]$ (−0.8 V vs. SCE) [1,2].

The events at more positive potential (0.71 and 0.81 V vs. SCE) were not defined, though it is obvious that some chemical reaction took place during the electrode reaction process.

3. Experimental

3.1. General procedures

All reactions were carried out under a nitrogen atmosphere using Schlenk techniques unless noted otherwise. Solvents were dried and degassed prior to use. $Mo(CO)_6$, *p*-Cl–C_6H_5SH, and dppm were obtained from Aldrich. Et_3N and I_2 were purchased from Shanghai Chemical Reagent Co. Elemental analyses were performed on a Carlo Erba MOD 1106. Infrared spectra (KBr pellets) were recorded on a Magna 750. UV-vis spectra were recorded on a Schimadzu UV-3000 (acetone was used as solvent). ^{1}H-, ^{13}C-, ^{31}P-, and ^{95}Mo-NMR spectra were measured on a Varian Unity-500 at 499.864, 125.708, 202.364 and 32.544 MHz, respectively. Proton and carbon chemical shifts are relative to internal acetone, that of phosphorus is relative to external aqueous saturated H_3PO_4 solution, and molybdenum's is relative to external aqueous 2 M Na_2MoO_4 solution.

Cyclic voltammetry (CV) measurements were carried out on a CV-1B from BAS (Bioanalytical Systems), using 0.10 M Et_4NBF_4 as the supporting electrolyte and acetone as solvent. The working electrode was glassy carbon (area 0.0804 cm^2), the auxiliary electrode was a platinum wire and the reference electrode was an

Table 5
Atomic coordinates ($\times 10^4$) and equivalent isotropic displacement parameters ($Å^2 \times 10^3$) for $\mathbf{2}\cdot CH_2Cl_2$

Atom	x	y	z	U_{eq}
Mo(1)	3279(1)	−4220(1)	2369(1)	36(1)
Mo(2)	4251(1)	−3189(1)	2468(1)	34(1)
S(1)	3402(1)	−3622(1)	1576(1)	42(1)
S(2)	4153(1)	−3886(1)	3252(1)	38(1)
S(3)	4724(1)	−2667(1)	1758(1)	38(1)
Cl(1)	4242(1)	−5480(1)	−77(1)	111(1)
Cl(2)	4129(2)	−1891(1)	5214(1)	124(1)
Cl(3)	5104(1)	550(1)	1532(1)	100(1)
P(1)	2443(1)	−4998(1)	1674(1)	44(1)
P(2)	2671(1)	−4926(1)	2839(1)	45(1)
O(1)	4286(2)	−5447(3)	2508(2)	71(1)
O(2)	2312(2)	−2990(3)	2323(2)	68(1)
O(3)	3823(2)	−2458(2)	2485(2)	43(1)
O(4)	5000	−3779(2)	2500	35(1)
C(0)	2049(3)	−5251(3)	2169(3)	54(2)
C(1)	3922(3)	−5004(3)	2440(3)	45(1)
C(2)	2658(3)	−3440(3)	2337(2)	45(1)
C(11)	3716(3)	−4118(3)	1138(2)	48(1)
C(12)	3385(4)	−4056(4)	556(3)	72(2)
C(13)	3552(5)	−4465(5)	177(3)	89(3)
C(14)	4054(4)	−4925(4)	385(3)	74(2)
C(15)	4412(3)	−4974(4)	963(3)	67(2)
C(16)	4244(3)	−4564(4)	1342(3)	56(2)
C(21)	4090(3)	−3308(3)	3778(2)	41(1)
C(22)	3529(3)	−2982(4)	3764(3)	66(2)
C(23)	3539(4)	−2552(4)	4207(3)	83(2)
C(24)	4109(4)	−2441(4)	4653(3)	71(2)
C(25)	4682(4)	−2752(4)	4687(3)	64(2)
C(26)	4663(3)	−3188(3)	4245(2)	50(2)
C(31)	4817(3)	−1747(3)	1725(2)	43(1)
C(32)	4410(3)	−1273(3)	1838(3)	63(2)
C(33)	4497(4)	−563(3)	1779(4)	72(2)
C(34)	4974(3)	−340(3)	1602(3)	60(2)
C(35)	5374(3)	−805(3)	1476(3)	55(2)
C(36)	5296(3)	−1511(3)	1539(3)	48(1)
C(41)	1792(3)	−4714(3)	1016(3)	55(2)
C(42)	1653(5)	−4019(5)	928(4)	118(4)
C(43)	1141(6)	−3792(6)	456(5)	182(7)
C(44)	777(6)	−4266(6)	50(5)	158(6)
C(45)	916(5)	−4940(5)	120(4)	111(3)
C(46)	1417(4)	−5172(4)	602(3)	79(2)
C(51)	2745(3)	−5799(3)	1471(3)	48(2)
C(52)	2923(4)	−5800(4)	1001(3)	68(2)
C(53)	3204(4)	−6369(4)	857(4)	83(2)
C(54)	3309(4)	−6961(4)	1192(4)	89(3)
C(55)	3141(4)	−6978(4)	1660(4)	85(2)
C(56)	2856(4)	−6397(4)	1804(3)	67(2)
C(61)	3012(3)	−5693(3)	3269(3)	56(2)
C(62)	2600(4)	−6232(4)	3308(3)	79(2)
C(63)	2854(6)	−6801(5)	3643(5)	106(3)
C(64)	3500(7)	−6844(5)	3949(5)	126(4)
C(65)	3920(5)	−6321(5)	3911(4)	116(4)
C(66)	3663(4)	−5743(4)	3572(3)	78(2)
C(71)	2219(3)	−4511(3)	3230(3)	58(2)
C(72)	2457(5)	−4530(5)	3798(4)	105(3)
C(73)	2131(9)	−4211(7)	4113(6)	148(5)
C(74)	1580(8)	−3876(6)	3834(7)	136(6)
C(75)	1332(5)	−3828(4)	3263(6)	111(4)
C(76)	1655(4)	−4144(4)	2949(4)	83(2)
Cl	172(3)	−2465(3)	2017(3)	252(3)
C	0	−1962(9)	2500	155(8)

aqueous SCE separated from the sample solution by a salt bridge containing 0.1 M Et_4NBF_4 in the solvent. Solutions were deoxygenated and blanketed with nitrogen. As a comparison, ferrocene was measured under identical conditions (as an internal potential standard). $E_{1/2} = +0.48$ V (vs. SCE) for the ferrocene–ferrocenium couple. The concentration of the sample compounds in these measurements was 10^{-3} M, the scan rate was 100 mV s^{-1}.

[Mo_2(μ-SC_6H_4–Cl-*p*)$_2$(CO)$_8$] was prepared referring to the literature method [1,2].

3.2. Syntheses of complexes *1* and *2*

(A) A sample of Mo_2(μ-SC_6H_4–Cl-*p*)$_2$(CO)$_8$ (0.705 g, 1 mmol) was dissolved in 30 ml of acetone resulting in green solution. To this green solution was added one equivalent Bu_4NBr (0.322 g, 1 mmol), the solution immediately turned brown, accompanied by a vigorous CO evolution. After 1 h of stirring, to the resulting solution was added one equivalent dppm (0.384 g, 1 mmol). After stirring overnight, the reaction solution was evaporated to 10 ml under vacuum and 20 ml of isopropanol was added, then this solution was filtered and the filtrate was allowed to stand at −4°C for several days. A black crystalline product **1** (0.72 g, yield ca. 70%) formed and was collected by filtration, washed with isopropanol, and dried in vacuum. Anal. Found: C, 49.60; H, 2.81. Anal. Calc. for $C_{43}H_{30}Cl_2Mo_2O_6P_2S_2$: C, 50.07; H, 2.93%; IR (KBr pellet): ν(CO) 2010(s), 1963(s), 1934(s), 1917(s) and 1884(s) cm^{-1}; ^{1}H-NMR (CD_3COCD_3): δ 2.9(d, 2H, P–CH_2–P) and 7.3–7.9 (m, 30H, SPh and PPh_2) ppm; ^{13}C-NMR (CD_3COCD_3): δ 232.2 (2CO, *trans* to P atom), 227.6 (4CO, *cis* to P atom), 136.4–129.4 (36C, SPh and PPh_2) and 55.1 (1C, P–CH_2–P); ^{31}P-NMR (CD_3COCD_3): δ 18.4 ppm; ^{95}Mo-NMR (CD_3COCD_3): δ −937 ppm and UV-vis (CD_3COCD_3): λ_{max} 444, 326 and 314 nm.

(B) To a green solution of Mo_2(μ-SC_6H_4–Cl-*p*)$_2$(CO)$_8$ (0.705 g, 1 mmol) in 30 ml of dichloromethane was added dppm (0.384 g, 1 mmol), and the solution gradually turned red–brown, accompanied by a CO evolution. After stirred overnight, the resulting solution was treated by the same way as in (A). **1** and an unexpected trace of red $\mathbf{2}\cdot CH_2Cl_2$ were obtained, and the trace $\mathbf{2}\cdot CH_2Cl_2$ as red crystals were separated from **1** by using a microscope in air. IR (KBr pellet): ν(CO) 1888(s) and 1869(s); ν(MoOMo), 748(m) and ν(Mo=O), 910(m) cm^{-1}. ^{31}P-NMR (CD_3COCD_3): δ 9.7 ppm.

3.3. X-ray crystallography

The crystals of **1** and $\mathbf{2}\cdot CH_2Cl_2$ were grown in acetone/isopropanol and CH_2Cl_2/isopropanol mixed solvents, respectively. Suitable crystal samples were

mounted on glass fibres on a Siemens SMART [12] area detector and using graphite-monochromated Mo–K_α X-radiation ($\lambda = 0.071073$ Å). Details of the crystal parameters, data collection and refinement are given in Table 3. Data were corrected for Lorentz and polarisation effects and for absorption effects by SADABS [13]. The structures were solved by conventional direct methods (SHELXTL) and were refined by the full-matrix least-squares method on all F^2 data using Silicon Graphics Indy computer [14]. All non-hydrogen atoms were refined anisotropically; hydrogen atoms were located at idealized positions and refined with fixed isotropic thermal parameters. Atomic coordinates are given in Tables 4 and 5.

Acknowledgements

We are grateful to NNSFC and SKLSC for financial support of this research work.

References

[1] B. Zhuang, J.W. McDonald, F.A. Schultz, W.E. Newton, Organometallics 3 (1984) 943.
[2] D.A. Smith, B. Zhuang, W.E. Newton, J.W. McDonald, F.A Schultz, Inorg. Chem. 26 (1987) 2524.
[3] B. Zhuang, L. Huang, L. He, Y. Yang, J. Lu, Acta Chim. Sin. 47 (1987) 25.
[4] B. Zhuang, G. Pan, L. Huang, Polyhedron 15 (1996) 3019.
[5] M. Minell, J.H. Enemark, R.T.C. Brownlee, M.J. O'Connor, A.G. Wedd, Coord. Chem. Rev. 68 (1985) 170.
[6] A. Nagasawa, Y. Sasaki, B. Wang, S. Ikari, T. Ito, Chem. Lett. (1987) 1271.
[7] B. Wang, Y. Sasaki, A. Nagasawa, T. Ito, J. Coord. Chem. 18 (1988) 45.
[8] (a) P. Maathur, S. Ghose, M.M. Hossain, P.B. Hitchcock, J.F. Nixon, J. Organomet. Chem. 542 (1997) 265. (b) J.I. Dulebohn, T.C. Stamatakos, D.L. Ward, D.G. Nocera, Polyhedron 10 (1991) 2813.
[9] (a) W.-Y. Yeh, Y.-J. Cheng, M.Y. Chiang, Organometallics 16 (1997) 918. (b) V. Riera, M.A. Ruiz, F. Villafañe, Organometallics 11 (1992) 2854.
[10] B. Zhuang, L. Huang, L. He, Chin. J. Struct. Chem. 14 (1995) 359.
[11] (a) D. Coucouvanis, A. Toupadakis, J.D. Lane, S.M. Koo, C.G. Kim, A. Hadjikyriacou, J. Am. Chem. Soc. 113 (1991) 5271. (b) S. Poder-Guillou, P. Schollhammer, F.Y. Pétillon, J. Talarmin, K.W. Muir, P. Baguley, Inorg. Chim. Acta 257 (1997) 153.
[12] SMART Software Reference Manual, Siemens Energy and Automation Inc., Madison, WI, 1994.
[13] G.M. Sheldrick, SADABS, Absorption Correction Program, University of Goeltingen, German, 1996.
[14] G.M. Sheldrick, SHELXTL 5.03, Siemens Analytical X-ray Instrument Inc., Madison, WI, 1990.